A Novel Variable Stiffness Soft Robotic Gripper

Dimuthu D. K. Arachchige[1], Yue Chen[2], Ian D. Walker[3], and Isuru S. Godage[1]

***Abstract*— Compliant grasping is crucial for secure handling objects not only vary in shapes but also in mechanical properties. We propose a novel soft robotic gripper with decoupled stiffness and shape control capability for performing adaptive grasping with minimum system complexity. The proposed soft fingers conform to object shapes facilitating the handling of objects of different types, shapes, and sizes. Each soft gripper finger has a length constraining mechanism (an articulable rigid backbone) and is powered by pneumatic muscle actuators. We derive the kinematic model of the gripper and use an empirical approach to simultaneously map input pressures to stiffness control and bending deformation of fingers. We use these mappings to demonstrate decoupled stiffness and shape (bending) control of various grasping configurations. We conduct tests to quantify the grip quality when holding objects as the gripper changes orientation, the ability to maintain the grip as the gripper is subjected to translational and rotational movements, and the external force perturbations required to release the object from the gripper under various stiffness and shape (bending) settings. The results validate the proposed gripper's performance and show how the decoupled stiffness and shape control can improve the grasping quality in soft robotic grippers.**

I. Introduction

Soft robots have higher flexibility and compliance than traditional rigid robots [1]–[4]. Research shows that soft robotic grippers can handle objects of various shapes and sizes and different object categories that are predominantly fragile and highly deformable [3]–[7]. Therefore soft robotic grippers present a promising path toward adaptive grasping, which can mimic the dexterity and versatility of biological appendages such as human hands. With rigid grippers, it is challenging to know the contact forces without added sensors, and therefore force control may be needed to prevent damages to objects. In addition, stiffness or compliance control of rigid grippers requires complex actuator-elastic element arrangement.

In contrast, soft robotic grippers are inherently compliant, conform to the environment, distribute contact forces, and, therefore, can facilitate compliant grasping without the need for actuator control based on complex sensor feedback. In addition, finger conformity improves the grip quality while stiffness control, if available, helps lock and maintain the finger deformation and, therefore, grip security. Further, the gripper may need to exert large forces on objects depending on the type, shape, and weight. Here, stiffness control enables it to withstand a range of external loads while preserving the grip. Moreover, stiffness control helps retain the payload without compromising dexterity in manipulation.

[1]Robotics and Medical Engineering Laboratory, School of Computing, DePaul University, Chicago, IL 60604. DARACHCH@depaul.edu [2]Dept. of Mechanical Engineering, University of Arkansas, Fayetteville, AR 72701. [3]Dept. of Electrical and Computer Engineering, Clemson University, Clemson, SC 29634.

This work is supported in part by the National Science Foundation Grants IIS-1718755, IIS-2008797, IIS-2048142, and DePaul University Academic Initiative Grant 602034.

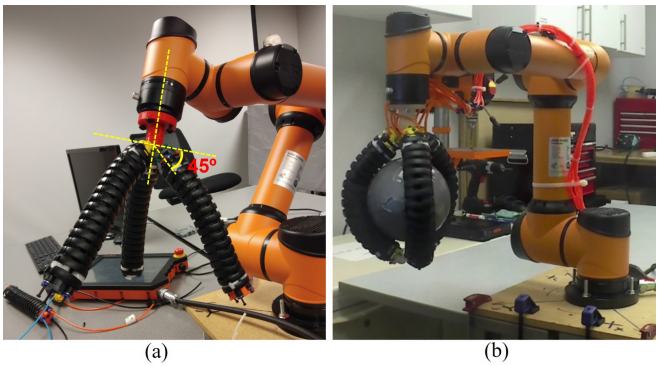

(a) (b)

Fig. 1: (a) Proposed tri-fingered soft robotic gripper attached as the end-effector of an AUBO-i5 industrial manipulator, (b) Gripper grasping a spherical object.

A. Previous Work

Many soft robotic grippers have been proposed to date. The work reported in [8] employs shape-memory alloys (SMA) and variable fluid viscosity to achieve variable stiffness. The authors of [9] and [10] used dielectric elastomer and low-melting-point alloy to create a variable stiffness gripper. Yang et al. [11] proposed a variable stiffness gripper with a built-in position feedback system. Similar actuation principle is reported in [8]. Given the low bandwidth of thermally activated materials, these grippers have limited dynamic stiffness control performance. Plus, dielectric elastomers require a high operating voltage and have low efficiency due to the need for heating and cooling and associated energy loss. Chen et al. [12] present a layer-jamming induced active vacuum adhesion gripper that can lift flat, concave, and convex-shaped objects. Here, a particle pack acts as a stiffness-changeable gripper that is susceptible to membrane damages. The 3D-printed soft gripper in [13] uses a combination of negative and positive pressures to vary the stiffness. The gripper reported in [14] inflates a portion of the soft finger to achieve stiffness control. Due to monolithic design, their actual force output makes them suitable for small-scale applications. In [15], a pangolin scales inspired layer with toothed pneumatic actuators is employed to control stiffness. The gripper design of [16] uses antagonistically arranged pneumatic muscle actuators (PMAs) to achieve the decoupled shape and stiffness variation. Further, the research

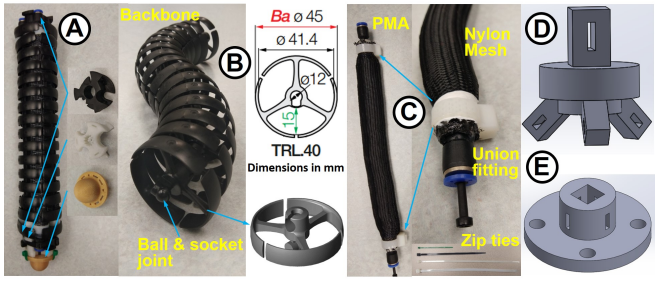

Fig. 2: (A) Assembled soft robotic finger, (B) length constraining mechanism, (C) A PMA, (D)-(E) CAD models of gripper base unit used to assemble fingers. (D) and (E) connect the gripper to AUBO-i5 6-DoF industrial robot.

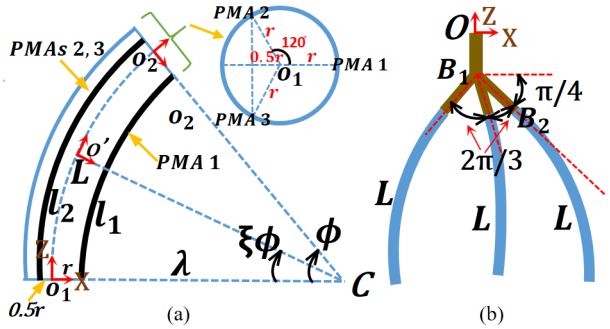

Fig. 3: (a) Schematic of the soft modular robotic finger, (b) Schematic of the gripper that uses three soft modular fingers.

in [16] uses a tendon-driven mechanism to apply forces to the fingers, which causes flexion and extension of the fingers. In [17], the gripper utilizes a screw and rod mechanism to complete the grasping operation, while PMAs control the stiffness. These mechanically driven grippers exhibit compliant grasping but have complex control schemes with low efficiency.

B. Contribution

We propose a novel pneumatically actuated soft robotic gripper (Fig. 1) with adaptive and decoupled stiffness and shape control capabilities to address these challenges. The soft fingers of the gripper utilize a length constraining mechanism to provide structural integrity and enable stiffness control while presenting a compliant environmental interface with minimum system complexity. The gripper fingers combine an articulable length constraining mechanism and PMAs to vary the finger stiffness that could be used for strong grips without trading compliance. The length constraining mechanism is inspired by the highly adaptable tails of the spider monkey [18]. Their tails can function as a manipulator for grasping tree branches while navigating the treetops, supporting structure while standing upright, or counterbalancing appendage when jumping and climbing. The tail's muscular lining actuates the skeletal structure (backbone or length constraining mechanism) underneath to obtain the desired structural shape (bending), stiffness, and strength during transformations between the aforementioned roles. Similar to their biological counterparts, we experimentally demonstrate that, when PMAs of the proposed gripper fingers are actuated, the length constraining mechanism offers structural shape, stiffness, and strength. We validate the gripper operation using three tests to assess the gripper efficacy, which shows that the proposed gripper can successfully grasp and maintain grips under various dynamic conditions.

II. Prototype Description

A. Gripper Design and Fabrication

1) Finger Design: The completed soft finger is shown in Fig. 2-A. It has two main components; an articulable length constraining mechanism (Fig. 2-B) and PMAs (Fig. 2-C). The length constrainer is a readily available robot dress pack manufactured by Igus Inc (part # Triflex R-TRL40). In the design, individual high tensile strength plastic units have been assembled to form an articulable kinematic chain. The individual units connected with ball-and-socket links allow free movement in multiple directions. We can 3D-print the same units for our purpose. However, it is rather cumbersome to 3D-print this complex unit. Thus, we decided to use the one available off the shelf. We decided on the finger length based on the length constrainer's bending capacity to form a 180°subtended angle. PMAs are anchored to the ends of the length constrainer using 3D-printed anchor units shown in Fig. 2-A. Extension mode PMAs are custom-made and 150 mm long. They can sustain pressures up to 700 kPa and extend by 50%. Fabrication steps of PMAs are presented in [19]. The inner diameter and thickness of the silicone PMA bladder tube are 11 mm and 2 mm, respectively. The length constrainer is radially symmetrically lined with three mechanically identical PMAs, push-to-connect fittings, 3D-printed finger end caps, and the wrapping of the whole unit (Fig. 2-A). A soft finger unit has an effective length of 180 mm and a diameter of 36 mm. The length constrainer limits the axial extension, and therefore a finger unit can only bend. The uniform arrangement of PMAs ensures circular arc-shaped bending within normal operating conditions. The length constrainer with PMAs helps achieve independent stiffness control through antagonistic muscle arrangement.

2) Gripper Fabrication: Our proposed gripper (Fig. 1) consists of three soft fingers in a symmetrical tri-fingered configuration to offer significant flexibility and versatility in handling different shapes of objects. The fingers are attached to a 3D-printed base unit shown in Fig. 2-D and E. The anchoring elements are designed at a $\frac{pi}{4}$ rad angle with respect to the horizontal plane (Figs. 1-a and 3-b). In fingers, we actuate two PMAs of the three simultaneously, which results in two effective DoF per finger. The reason for this decision is threefold; (1) obtain bidirectional bending using extension mode PMAs in an antagonistic arrangement, (2) strong gripper force generation with simultaneous actuation of 2 PMAs to generate twice as much bending torque, and (3) achieve stiffness control with the remaining PMA. Therefore, this gripper design allows us to generate more gripping torque while decoupling stiffness and shape control. In the proposed gripper design, we simultaneously actuate all three fingers, and thus the gripper has two DoF in total.

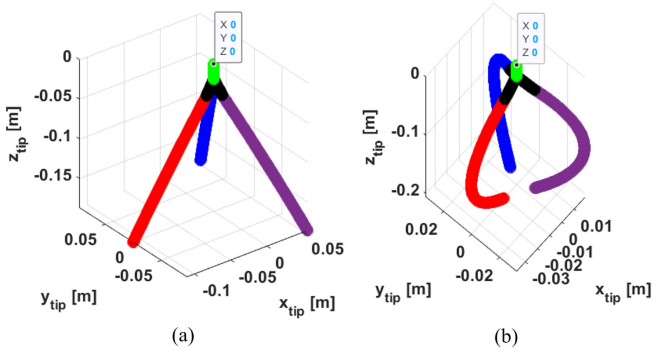

Fig. 4: Illustration of the forward kinematics model: (a) at natural pose with straight soft finger modules without grasping an object (b) grasping operation of an object by simultaneously bending soft finger modules.

III. System Modeling

A. Kinematic Model

Fig. 3-a shows the schematic of the soft finger. The finger base is positioned at the origin of the robot coordinate frame such that one PMA is on the X axis and the length change of this is l_1. Thus, upon actuation, the finger bends on the X-Z plane. Noting prior work, we assume that the finger unit bends in a circular arc shape [20], [21]. The three PMAs are placed on a circular rigid frame at a radius r from the center and $\frac{2\pi}{3}$ rads apart inside the inextensible rigid length constrainer (Fig. 3-a). Thus, actuation points of PMAs form an equilateral triangle of side $r\sqrt{3}$. With that, when one PMA (PMA 1) forms a r distance along the X axis from the length constrainer's center, the remaining two PMAs (PMAs 2 & 3) form $\frac{r}{2}$ distance along the -X-axis from the origin of the robot coordinate system. L_0 denotes the initial length of the PMAs and, $l_i \in \mathbb{R}$ is the length variation where $l_{i:min} \leq l_i(t) \leq l_{i:max}$ for $i \in \{1,\ 2\}$ and t denotes the actuator number and time, respectively. Thus, $L_i(t) = L_0 + l_i(t)$ presents the length of each actuator at time t. The work reported in [22] presented curve parameters that define the spatial position and orientation of a single section extensible continuum arm in 3D taskspace. We can extend the derivation of [23], [24] to obtain model kinematics of an inextensible soft finger module in planar taskspace. Let the joint variable vector be $q = [l_1(t),\ l_2(t)]^T$. Two spatial parameters can describe the finger bending arc, the radius of curvature, $\lambda \in (0, \infty)$ with instantaneous center C, and the angle subtended by the arc, $\phi \in (0, \pi)$. Using arc geometry and applying the inextensible constraint, $L = \lambda\ \phi$, we can relate q and curve parameters as

$$L + l_1 = (\lambda - r)\,\phi \Rightarrow l_2 = -r\phi \tag{1}$$

$$L + l_2 = \left(\lambda + \frac{r}{2}\right)\phi \Rightarrow l_2 = \frac{\phi r}{2} \tag{2}$$

Noting the PMAs are of extension type and assuming input pressure of PMAs is proportional to their length, we can define ϕ as

$$\phi = \begin{cases} \frac{-l_1}{r} & ;l_1 > l_2 \text{ or } P_1 > P_2 \\ \frac{2l_2}{r} & ;l_1 \leq l_2 \text{ or } P_1 \leq P_2 \end{cases} \tag{3}$$

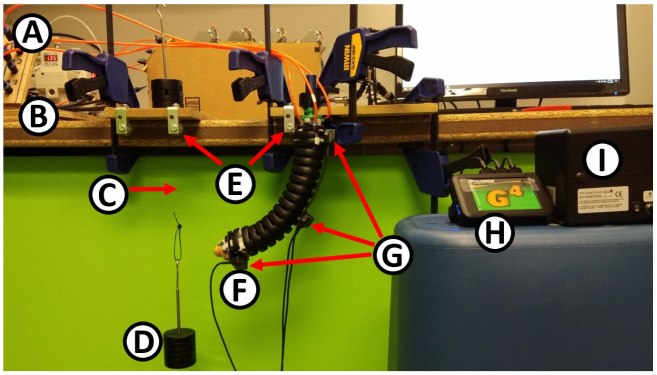

Fig. 5: Experiment setup to map bending stiffness, finger shape, and actuation pressure: (A) pressure distribution tubes, (B) proportional digital pressure controllers, (C) Nylon string, (D) load, (E) pulleys, (F) soft robotic finger unit, (G) tracking sensor probes, (H) tracking source, (I) wireless communication hub of the Polhemus G4 wireless magnetic tracking system.

where P_i is the pressure input to the i^{th} PMA and $\lambda = \frac{L}{\phi}$. Note that, gripping action only involves the scenario $P_1 \leq P_2$. Employing the curve parameters, the homogeneous transformation matrix (HTM) can be derived as [23]

$$\begin{aligned} \mathbf{T}(c,\xi) &= \mathbf{P}_x(\lambda)\ \mathbf{R}_y(\xi\phi)\ \mathbf{P}_x(-\lambda) \\ &= \begin{bmatrix} \mathbf{R}(q,\xi) & \mathbf{p}(q,\xi) \\ \mathbf{0}_{1x3} & \mathbf{1} \end{bmatrix} \end{aligned} \tag{4}$$

where $\mathbf{R}_y \in \mathbb{SO}^2$ and $\mathbf{P}_x \in \mathbb{R}$ are the homogeneous rotation matrices about Y and translation matrix along the X axes. The scalar ξ defines any point along the length constrainer. $\mathbf{R} \in \mathbb{SO}^2$ and $\mathbf{p} = [x,\ z]^T \in \mathbb{R}^2$ denote the rotation and position matrices of the robot finger, respectively. Refer to [23] for more details on the derivation. The top unit of the gripper is at the origin of the coordinate frame $\{O\}$ as shown in Fig. 3-b. To derive the kinematic model of the entire gripper, the following translations and rotations are applied.

$$\begin{aligned} &\mathbf{T}_1 = \mathbf{P}_Z(\sigma)\,\mathbf{R}_Y(3\pi/4)\,\mathbf{T}(q,\xi) \\ &\mathbf{T}_2 = \mathbf{R}_Z(2\pi/3)\,\mathbf{T}_1 \text{ and } \mathbf{T}_3 = \mathbf{R}_Z(4\pi/3)\,\mathbf{T}_1 \end{aligned}$$

where $\mathbf{T}_1$ is the HTM of the i^{th} finger, and $\mathbf{R}_z$ is the homogeneous rotation matrix about the Z axis. The forward kinematics can be used to illustrate gripper operation in the taskspace, as shown in Fig. 4.

B. Map Actuation Pressure, Stiffness, and Shape

We experimented with mapping the finger shape to PMA pressure combinations. We used the experimental setup shown in Fig. 5 to obtain a rich set of data related to shape variation against the actuation pressure combinations. Here, we applied a range of actuation pressures under no-load conditions. At each pressure amount, we recorded the bending angle (ϕ) of the finger using a position and orientation tracking sensor [25].

Fig. 6-a shows how bending angle, ϕ, varies per input pressure combinations. To experiment with the effect of shape and stiffness control, we extract pressure combinations with the same ϕ. We achieve this by considering planes

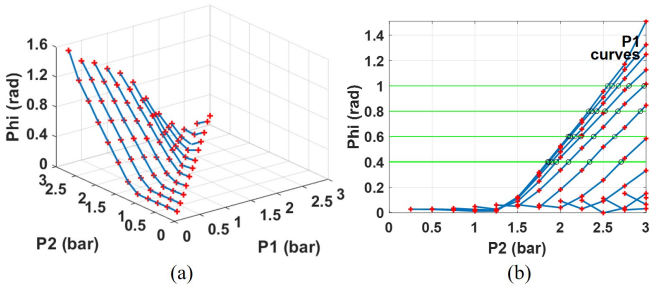

(a) (b)

Fig. 6: (a) Bending shape variation of a finger, (b) Use the shape-pressure mapping to find four different stiffness values associated with the same bending angle, ϕ.

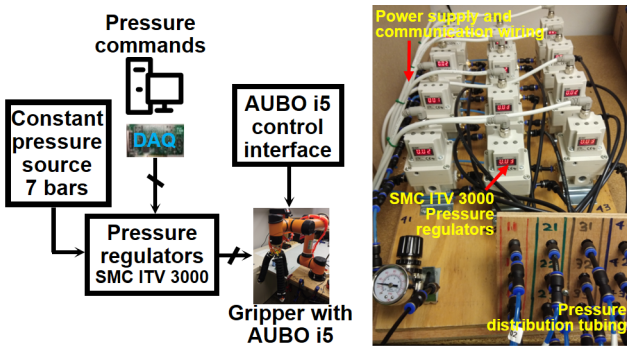

(a) (b)

Fig. 7: (a) Gripper operation experimental setup block diagram. (b) Pressure regulator assembly that controls the bending of soft finger modules.

at different ϕ values and interpolating the pressure combinations that result in the desired ϕ, as shown in Fig. 6-b. The first three columns of Table I detail the identified ϕ values and the pressure combinations. Next, we used the same experiment set up in Fig. 5 to obtain stiffness values for the identified ϕ values and pressure combinations. Here, we applied identified actuation pressures under no-load and fixed-load conditions. At each pressure combination, we recorded the bending angle, change in bending angle ($\Delta\phi$) of the finger, and the torque loading ($\Delta\tau$) that caused the bending angle perturbation. We applied the load profiles using a pulley arrangement so that torque perturbation is normal to the gripper finger unit's neutral axis. Then we calculated the bending stiffness using $K = \frac{\Delta\tau}{\Delta\phi}$ as presented in the final column of Table I. The resulting stiffness variation indicates that the bending stiffness increases when the common-mode actuation pressure increases in the PMAs. It is clear that we can obtain the same bending angle for different combinations of P_1 and P_2 but with different stiffness values indicating the decoupled shape and stiffness control capability. The shape-stiffness mapping will be used to validate the gripper in the next section, experimentally.

IV. Experimental Validation

A. Experimental Setup

The overall gripper operation is illustrated in Fig. 7-a. The setup's input pressure is a constant 7 bar pressure, supplied by a central pneumatic air compressor. It is distributed to SMC ITV3000 series electro-pneumatic pressure regulators shown in Fig. 7-b. PMAs of the gripper fingers are connected to two pressure regulators to control the bending (the bundled two-PMAs) and stiffness (the remaining PMA). The pressure commands are generated by a Matlab Simulink Desktop Real-time model and communicated via a National Instrument DAQ card. To validate the gripper, we attach the gripper base to the end of an AUBO-i5 [26] industrial robot via a custom-designed unit (Fig. 2-E). The AUBO-i5 robot manipulator has 6-DoF with maximum joint speeds up to 29.7 rpm and is controlled by programs developed using AUBORPE software [26].

B. Testing Methodology

We define the grip quality by three metrics: 1) holding ability as the gripper changes orientation, 2) maintaining the grip as the gripper moves, and 3) the amount of force required to release the object from the grip. We conducted three tests to validate each of these qualities, namely orientation test, velocity test, and force test. We used three different object shapes, sphere, box, and pyramid. We selected object shapes to have smooth surfaces as well as a combination of geometrically varying surfaces. We lined the finger surfaces with sandpaper to improve the grip. We cover the object surfaces with the same material in order to provide a uniform friction coefficient. The object sizes were determined based on the finger dimensions. Each object's largest dimension (box, pyramid edge lengths, and sphere diameter) is approximately similar to the finger length. Each object weighs about 100 g. Table I provides details on required pressure combinations to obtain sixteen different stiffness values while keeping the finger shape constant on four different occasions. We conducted each orientation, velocity, and force test under sixteen shape-stiffness variations. The experiments are repeated for all the objects.

C. Orientation Test

The orientation test was planned to present how the gripper can handle objects with different profiles and shapes against gravity and rotational motions. In practical operations, robots have to reorient payloads. Hence a gripper should be able

TABLE I: Mapping finger shapes, pressure, and stiffness values

Finger shape [ϕ (rad)]	**Pressure combinations**		**Bending stiffness** (Nm/ rad)
	P1 (bar)	**P2** (bar)	
0.4	0.50	1.86	0.63
	0.75	1.90	0.81
	1.00	1.96	1.11
	1.25	2.09	1.32
0.6	0.50	2.11	0.71
	0.75	2.17	0.85
	1.00	2.24	1.40
	1.25	2.39	1.71
0.8	0.50	2.36	0.86
	0.75	2.42	1.42
	1.00	2.52	1.90
	1.25	2.67	2.18
1.0	0.50	2.60	1.56
	0.75	2.68	1.98
	1.00	2.80	2.33
	1.25	2.98	2.58

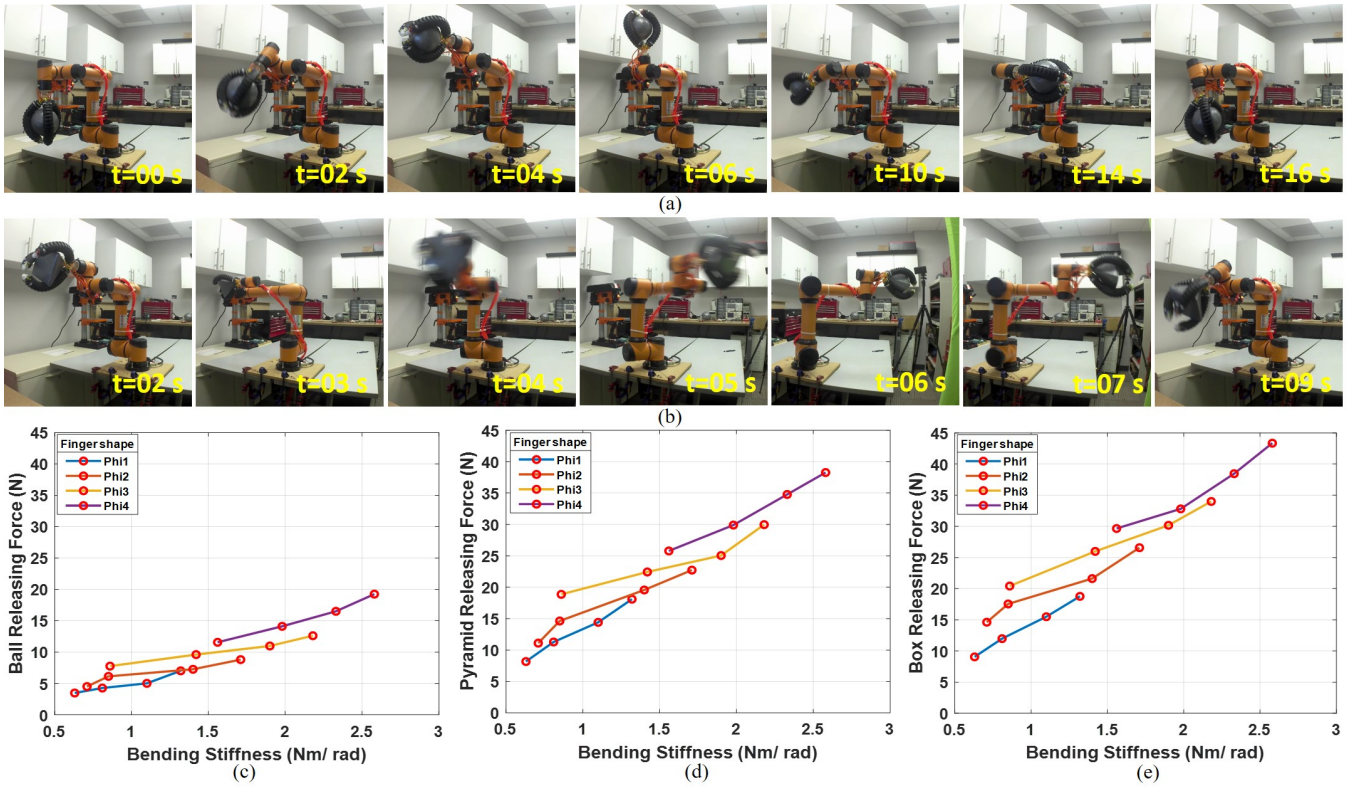

Fig. 8: (a) Orientation test sequences for the sphere object. (b) The velocity test sequences for the pyramid objects. (c)-(d)-(e) The force test results for sphere, pyramid, and box object failure forces. Here, the finger shape denotes the finger bending angles.

to reorient objects. In this experiment, we move a grasped object from one orientation to another using the two end-effector joints of the manipulator robot running at 15 rpm. A series of images related to the orientation test on a spherical object is shown in Fig. 8-a. For all objects, the gripper showed firm grasping without failure under all stiffness variations. Therefore, the successful handing of objects with no quantitative difference shows that our gripper design is robust in orientation tasks.

D. Velocity Test

A gripper's ability to handle linear velocity dictates how fast the robot can complete the handling job, i.e., pick and place operation. Thus, to improve productivity, a gripper should be able to handle payloads at higher velocities. In this test, the robot arm is used to grasp an object and move from one place to another at a relatively high linear velocity while maintaining the gripper orientation. The velocity test steps of the pyramid-shaped object are presented in Fig. 8-b. First, the pyramid is grasped at a pre-programmed home position of the AUBO-i5 robot. Next, a linear trajectory is executed. Similar to the orientation test, we conducted the velocity test for all three objects. The gripper showed a firm object holding under all stiffness variations at the maximum moving velocity. Therefore, the successful handling of objects with no quantitative difference shows that the proposed gripper is robust in velocity handling. The accompanying video submission includes the results of orientation and velocity tests under sixteen stiffness settings.

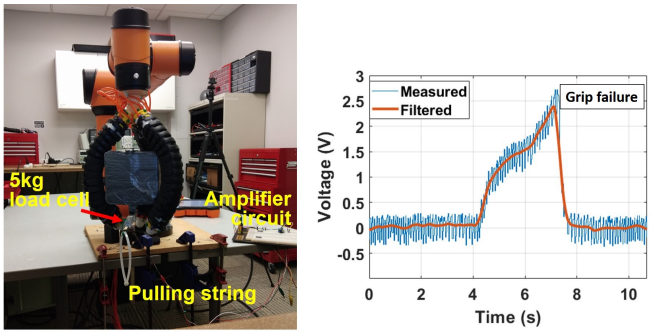

Fig. 9: (a) Force test experiment, (b) Maximum failure force measurement. The force is increased until the grip failed.

E. External Force Perturbation Test

The force test is designed to measure the effect of stiffness change quantitatively. In this test, a pulling force is applied until the object released from the grip. Fig. 9-a shows how the force test is conducted on the box-shaped object. We used a 5 kg load cell coupled with an instrumentation amplifier to measure the pulling force exerted on the object. First, we calibrated the load cell to read standard force values based on voltage readings. The load cell was firmly attached to the object so that a vertical downward force can be applied until the grip fails. Fig. 9-b illustrates a typical reading recorded during a pulling action. We used a moving average filter to filter noisy data and obtain the force when the grip fails. Similar to the previous two tests, we conducted the force

test for all three objects under the four finger bending angles. Altogether, the releasing force was measured under sixteen stiffness variations. Measured maximum forces against the stiffness variation for each object are presented in Fig. 8-c. The data shows that, for the same finger shape (i.e., bending angle, ϕ), high stiffness grasping resulted in high grip failure forces. Similarly, higher bending angles (i.e., firmer grip), resulted in high grip failure forces. Among the objects used in the experiments, the sphere object has relatively smoother contours than the pyramid and box surfaces (i.e., no edges). Therefore, the sphere's failure force at each finger shape shows a relatively lower value than that of the pyramid and the box. The box has the largest geometrically irregular shape, which resulted in the highest failure forces. The results show that the proposed soft gripper with independent shape and stiffness control can complete various grasping tasks under challenging conditions. It should be noted that when the gripper is in a grasping configuration fingers may show different stiffness values depending on the object shape. This stiffness variation is one of the key features of the proposed soft gripper.

V. Conclusion

Due to inherent compliance and conforming capability, soft robotic grippers present a promising path toward adaptive grasping. We hypothesized that independent shape and stiffness control can improve the grasping operation and grip quality. This paper proposed a novel soft robotic gripper based on an inextensible finger design with independent shape and stiffness control. We detailed the proposed soft finger design and how the use of a length constraining mechanism improves structural integrity and facilitates independent shape and stiffness control. The kinematic models of soft fingers and the gripper were derived and validated. For better accuracy, we utilized empirical data gathered from rigorous testing to control shape and stiffness. We conducted three tests to show the effectiveness of the proposed soft robotic gripper. The tests demonstrated the gripper's ability to sustain rotational and linear motion with grasped objects. The force test showed that the stiffness control could be used to improve the grasping quality.

References

[1] Y. Chen, L. Wang, K. Galloway, I. Godage, N. Simaan, and E. Barth, "Modal-based kinematics and contact detection of soft robots," *Soft Robotics*, 2020.

[2] K. C. Galloway, Y. Chen, E. Templeton, B. Rife, I. S. Godage, and E. J. Barth, "Fiber optic shape sensing for soft robotics," *Soft robotics*, vol. 6, no. 5, pp. 671–684, 2019.

[3] J. Shintake, V. Cacucciolo, D. Floreano, and H. Shea, "Soft robotic grippers," *Advanced Materials*, vol. 30, no. 29, p. 1707035, 2018.

[4] J. Walker, T. Zidek, C. Harbel, S. Yoon, F. S. Strickland, S. Kumar, and M. Shin, "Soft robotics: A review of recent developments of pneumatic soft actuators," in *Actuators*, vol. 9, no. 1. Multidisciplinary Digital Publishing Institute, 2020, p. 3.

[5] M. Manti, T. Hassan, G. Passetti, N. D'Elia, C. Laschi, and M. Cianchetti, "A bioinspired soft robotic gripper for adaptable and effective grasping," *Soft Robotics*, vol. 2, no. 3, pp. 107–116, 2015.

[6] J. Zhou, S. Chen, and Z. Wang, "A soft-robotic gripper with enhanced object adaptation and grasping reliability," *IEEE Robotics and automation letters*, vol. 2, no. 4, pp. 2287–2293, 2017.

[7] J. Chenl, H. Deng, W. Chai, J. Xiong, and Z. Xia, "Manipulation task simulation of a soft pneumatic gripper using ros and gazebo," in *2018 IEEE International Conference on Real-time Computing and Robotics (RCAR)*. IEEE, 2018, pp. 378–383.

[8] M. Liu, L. Hao, W. Zhang, and Z. Zhao, "A novel design of shape-memory alloy-based soft robotic gripper with variable stiffness," *International Journal of Advanced Robotic Systems*, vol. 17, no. 1, p. 1729881420907813, 2020.

[9] J. Shintake, B. Schubert, S. Rosset, H. Shea, and D. Floreano, "Variable stiffness actuator for soft robotics using dielectric elastomer and low-melting-point alloy," in *2015 IEEE/RSJ International Conference on Intelligent Robots and Systems (IROS)*. IEEE, 2015, pp. 1097–1102.

[10] J. Yan, H. Zhang, P. Shi, X. Zhang, and J. Zhao, "Design and fabrication of a variable stiffness soft pneumatic humanoid finger actuator," in *2018 IEEE International Conference on Information and Automation (ICIA)*. IEEE, 2018, pp. 1174–1179.

[11] Y. Yang, Y. Chen, Y. Li, Z. Wang, and Y. Li, "Novel variable-stiffness robotic fingers with built-in position feedback," *Soft robotics*, vol. 4, no. 4, pp. 338–352, 2017.

[12] R. Chen, L. Wu, Y. Sun, J. Chen, and J. Guo, "Variable stiffness soft pneumatic grippers augmented with active vacuum adhesion," *Smart Materials and Structures*, 2020.

[13] R. Mutlu, C. Tawk, G. Alici, and E. Sariyildiz, "A 3d printed monolithic soft gripper with adjustable stiffness," in *IECON 2017-43rd Annual Conference of the IEEE Industrial Electronics Society*. IEEE, 2017, pp. 6235–6240.

[14] Z. Wang and S. Hirai, "A soft gripper with adjustable stiffness and variable working length for handling food material," in *2018 IEEE International Conference on Real-time Computing and Robotics (RCAR)*. IEEE, 2018, pp. 25–29.

[15] T. Sun, Y. Chen, T. Han, C. Jiao, B. Lian, and Y. Song, "A soft gripper with variable stiffness inspired by pangolin scales, toothed pneumatic actuator and autonomous controller," *Robotics and Computer-Integrated Manufacturing*, vol. 61, p. 101848, 2020.

[16] L. A. Al Abeach, S. Nefti-Meziani, and S. Davis, "Design of a variable stiffness soft dexterous gripper," *Soft robotics*, vol. 4, no. 3, pp. 274–284, 2017.

[17] Z. Tang, J. Lu, Z. Wang, and G. Ma, "The development of a new variable stiffness soft gripper," *International Journal of Advanced Robotic Systems*, vol. 16, no. 5, p. 1729881419879824, 2019.

[18] P. Lemelin, "Comparative and functional myology of the prehensile tail in new world monkeys," *Journal of Morphology*, vol. 224, no. 3, pp. 351–368, 1995.

[19] I. S. Godage, D. T. Branson, E. Guglielmino, and D. G. Caldwell, "Pneumatic muscle actuated continuum arms: Modelling and experimental assessment," in *2012 IEEE International Conference on Robotics and Automation*. IEEE, 2012, pp. 4980–4985.

[20] A. A. Nazari, D. Castro, and I. S. Godage, "Forward and inverse kinematics of a single section inextensible continuum arm," *arXiv preprint arXiv:1907.06518*, 2019.

[21] J. Deng, B. H. Meng, I. Kanj, and I. S. Godage, "Near-optimal smooth path planning for multisection continuum arms," in *2019 2nd IEEE International Conference on Soft Robotics (RoboSoft)*. IEEE, 2019, pp. 416–421.

[22] I. S. Godage, D. T. Branson, E. Guglielmino, G. A. Medrano-Cerda, and D. G. Caldwell, "Shape function-based kinematics and dynamics for variable length continuum robotic arms," in *2011 IEEE International Conference on Robotics and Automation*. IEEE, 2011, pp. 452–457.

[23] I. S. Godage, G. A. Medrano-Cerda, D. T. Branson, E. Guglielmino, and D. G. Caldwell, "Modal kinematics for multisection continuum arms," *Bioinspiration & biomimetics*, vol. 10, no. 3, p. 035002, 2015.

[24] ——, "Dynamics for variable length multisection continuum arms," *The International Journal of Robotics Research*, vol. 35, no. 6, pp. 695–722, 2016.

[25] Polhemus, *Polhemus G4 User Manual*, urm10ph238 ed., Alken, Inc. dba Polhemus, https://polhemus.com/assets/img/G4-User-Manual-URM10PH238-D.pdf, jul 2013.

[26] A. Robotics, *AUBO–i5 User Manual*, 4th ed., AUBO (Beijing) Robotics Technology Co., Ltd, https://www.robots.ch/downloads/AUBO-i5-MANUALV4.3-v11.pdf, 2019.